Chemical Engineering Science 270 (2023) 118539

Contents lists available at ScienceDirect

Chemical Engineering Science

journal homepage: www.elsevier.com/locate/ces

Xenon hydrate formation in water-in-oil emulsion: Investigation with the radiographic method

Andrey Yu. Manakov [a,b,*], Konstantin E. Kuper [c,d], Arkadi N. Drobchik [e], Alexey K. Sagidullin [a,b], Matvei E. Semenov [b,f], Andrey S. Stoporev [a,b]

[a] Nikolaev Institute of Inorganic Chemistry SB RAS, Ac. Lavrentiev ave., 3, 630090 Novosibirsk, Russian Federation
[b] Department of Petroleum Engineering, Kazan Federal University, Kremlevskaya str, 18, 420008 Kazan, Russian Federation
[c] Budker Institute of Nuclear Physics of SB RAS, Lavrentiev ave., 11, 630090 Novosibirsk, Russian Federation
[d] Synchrotron Radiation Facility SKIF, Boreskov Institute of Catalysis, Nikol'skiy ave, 1, 630559 Kol'tsovo, Russian Federation
[e] Trofimuk Institute of Petroleum Geology and Geophysics SB RAS, Ac. Koptyug ave., 3, 630090 Novosibirsk, Russian Federation
[f] Institute of Oil and Gas Problems SB RAS, Oktyabrskaya str, 1, 677890 Yakutsk, Russian Federation

HIGHLIGHTS

- Xenon hydrate formation in water in oil emulsion was studied by radiographic method.
- Hydrate formation follows two stages.
- The first stage is the rapid growth of the hydrate crust at the gas – emulsion interface.
- The second stage is slow hydrate growth throughout the emulsion.
- Hydrate formation results in mechanical deformation of the emulsion sample.

ARTICLE INFO

Article history:
Received 6 December 2022
Received in revised form 20 January 2023
Accepted 31 January 2023
Available online 03 February 2023

Keywords:
Gas hydrate
Oil
Xenon
Emulsion
Radiography
DSC

ABSTRACT

Formation of gas hydrate plugs can significantly complicate oil recovery. For this reason, investigating hydrate formation in oil disperse systems is topical. This work presents the results of radiographic and DSC investigations of xenon hydrate formation in a water-in-oil emulsion. The process proceeds in two stages as follows. The hydrate proliferates near the emulsion–gas boundary in the first stage. The hydrate particles in this region grow together, at least partially. The final hydrate content in this area is significantly higher than in other parts of the sample. In the second stage, the hydrate's slow growth occurs over the sample's entire volume distorting its shape, possibly due to the difference in water and hydrate molar volumes. At this stage, a significant part of the hydrate (33%) forms with no detectable heat release. The obtained results will improve the description of the kinetics of hydrate growth in static water-in-oil emulsions.

1. Introduction

Gas hydrates are widespread and are one of the promising non-conventional sources of natural gas. Detailed information on the natural gas hydrates and the physical chemistry of these compounds may be found in (Hassanpouryouzband et al., 2020; Manakov and Stoporev, 2021; Sloan and Koh, 2007). In the gas and petroleum industry, the formation of technogenic gas hydrates leads to the clogging of boreholes and industrial pipelines, which may result in emergency accidents with various consequences (Aman and Koh, 2016; Sloan et al., 2010). In the case of oil production, hydrate formation proceeds on water droplets dispersed in oil. The coalescence of the formed hydrate particles leads to the hydrate plug formation (Aman and Koh, 2016; Hu and Koh, 2017). The peculiarities of hydrate formation in such systems discovered in laboratory studies can help to explain the behavior of real systems. Thus, investigating hydrate formation in oil dispersions is relivent, which drives the interest in conducting a more detailed study in this area.

The essential features of gas hydrate formation from water in oil emulsions have been studied in (Turner et al., 2009a,2009b). It was

* Corresponding author at: Nikolaev Institute of Inorganic Chemistry SB RAS, Ac. Lavrentiev ave. 3, 630090 Novosibirsk, Russian Federation.
E-mail addresses: manakov@niic.nsc.ru (A.Yu. Manakov), K.E.Kuper@inp.nsk.su (K.E. Kuper), a.n.drobchik@gmail.com (A.N. Drobchik), sagidullin@niic.nsc.ru (A.K. Sagidullin), stopor89@bk.ru (A.S. Stoporev).

https://doi.org/10.1016/j.ces.2023.118539
0009-2509/

demonstrated that hydrate first occurs at the water – oil boundary, forming a spherical shell around a water drop. The size of the majority of water drops in the emulsion does not change, though a small admixture of particles 2–3 times larger than the initial ones appears. Hydrate is formed from the gas dissolved in oil. The formation of hydrates at the water – oil boundary differs from the processes occurring at the interface between water and hydrate-forming gas (see a recent review (Zhang et al., 2022)). Simplifying the situation, we can say that paraffins and asphaltenes can form shells on liquid droplets. This decreases the physical surface of the liquid available for hydrate formation and slows down the interphase mass transfer. All these factors retards the hydrate formation oil dispersions. On the other hand, solid particles (predominantly asphaltenes) can serve as centers of hydrate nucleation facilitating hydrate formation.

Further growth of hydrate proceeds from water present under the hydrate shell, due to gas diffusion through the hydrate layer. Two mechanisms of hydrate formation from the drops in an emulsion have been proposed: (a) according to the independent microreactor model and (b) relay crystallization. In the independent microreactor model, hydrate nucleation and growth proceed singly for each water drop in the emulsion. Both mechanisms are applied for static and mixing conditions (Turner et al., 2009a,2009b; Avendaño-Gómez et al., 2006; Dalmazzone et al., 2009). The relay mechanism involves the transfer of hydrate formation over the dispersion volume due to secondary nucleation upon contact of a water drop with a particle on which the hydrate shell already has been formed. In this case, the drop and the particle do not necessarily merge. A model implying rapid hydrate formation according to the relay mechanism in a part of the emulsion, followed by slower hydrate formation in the sample's other sections, is based on calorimetric data on hydrate formation in static emulsions (Semenov et al., 2015; Stoporev et al., 2019). Experimental studies and modeling of hydrate growth in stirred water in oil emulsions are described in Lv et al. (2016). A conceptual model providing two-stage hydrate formation in emulsions is proposed: (a) formation of the spherical hydrate shells on the drops in emulsion, (b) junction of the drops and destruction of shells proceeding due to the collisions between particles. As a result, a complicated mixture of water and hydrate is formed with a part of water encapsulating inside hydrate shells. Experiments have shown that particle size increases by a factor of about two during the reaction, and particle size changes rapidly only at the start of the hydrate formation process. In Lv et al. (2020), a universal kinetic model describing hydrate formation in water-in-oil emulsions for multiphase flows was proposed. The primary hydrate nucleation is assumed to occur only on a few water drops. Then nucleation propagates according to the relay mechanism over a definite number of neighboring drops (up to 20% of the total). Finally, it was demonstrated that the content of coarse particles in the emulsion increases during hydrate formation while the part of small particles decreases (Wu et al., 2020). Thus, the average particle size increases. The water to hydrate transformation degree decreases with an increase in water content, which may be due to the capture of water drops into the agglomerates of particles. With water content up to 40%, hydrate suspension forms, while at 50% the particles stick together. It may be stressed that almost all the models considered above are speculative to a substantial extent because direct visualization of hydrate formation in oil suspensions is presently impossible. For this reason, there is still no distinctness in understanding the mechanism of hydrate formation in the emulsion. This is especially true for the static conditions, when there are no mutual collisions of drops/particles in the emulsion/suspension.

It is well known that xenon is used in many high-tech areas of industry and science (Pyae et al., 2015; Uhm et al., 2008), as well as in medicine (Xia et al., 2018). Currently, xenon is extracted from the distillation of liquefied air, which causes its high price. In this regard, at present, an urgent task is to obtain it from natural gas (Smetannikov et al., 2010; Petukhov et al., 2022). The combined methods proposed for this include the use of gas hydrates for the enrichment of gas mixtures with xenon (Sergeeva et al., 2021). Xenon forms a gas hydrate of the same structural type as methane (Manakov and Stoporev, 2021), but xenon hydrate is more stable. Thus, at a temperature of about 0 °C, the equilibrium pressure of methane over methane hydrate is 2.51 MPa, and that of xenon over xenon hydrate is 0.15 MPa; at a xenon pressure of 0.1 MPa, the equilibrium temperature of xenon hydrate is −10 °C (Istomin and Yakushev, 1992). The heat of decomposition of xenon hydrate with the composition $Xe{\cdot}5.9H_2O$ to water and xenon gas is 62 kJ/mol (Handa, 1986).

X-ray tomography and radiography have been successfully implemented to investigate gas hydrate formation in ice – hydrate-former disperse systems. These methods were applied to observe the nucleation and growth of xenon hydrate on the ice spheres (Zhao et al., 2020) and water drops (Liang et al., 2021). The formation of cyclopentane hydrate in cesium salt solution was visualized with the help of radiography and tomography, as described in (Pillers and Heindel, 2021). The authors of (Le et al., 2020) studied the formation of methane hydrate in sand from the potassium iodide solution, which was taken as a contrast. In the present work, we describe the first results of visualization of the xenon hydrate formation in a water-in-oil emulsion, employing the radiographic method.

2. Materials and methods

99.95% pure xenon, distilled water, and oil from a West Siberian oil field were used in the work. Oil's composition and characteristics were as following: asphaltenes, 5.7 wt%; resins, 12.1 wt%; paraffins, 3.4 wt% and balance saturates + aromatic, density 0.876 kg/m^3, viscosity 37.1 mPa/s, pour point −15.5 °C. Density and viscosity were determined at 20 °C. The experiments were carried out with a 50 wt% water-in-oil emulsion. The emulsion was prepared with the help of a manual mixer (800 rpm, 20 min). The procedure for preparing the emulsion was chosen by trial and error in such a way as to ensure the preparation of the most stable emulsion. The resulting emulsions were stable for at least six months. According to optical microscopy data, the average size

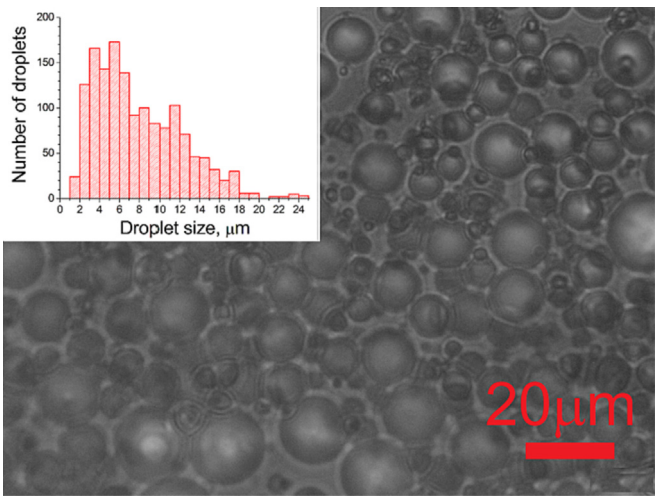

Fig. 1. Photo of the emulsion used. The droplet size distribution is shown in the inset.

of drops in the emulsion was 7.7 μm, size range was 1.6 – 24.7 μm (Fig. 1).

Experiments were carried out at the Microscopy and Tomography Synchrotron Radiation Station at VEPP-3 (Institute of Nuclear Physics SB RAS, Novosibirsk). The radiographic recording was carried out using Ni-filtered (100 μm) polychromatic synchrotron radiation (below referred to as SR). The energy spectrum of SR expanded from 25 to 60 keV with the maximum around 45 keV. The electron orbit stability in the VEPP-3 storage ring (50 μm), the small size of the SR source (0.5x1.5 mm^2) and a large distance from the radiation source point to the sample (16.5 m) allowed the acceptable spatial resolution of radiography to be achieved. The X-ray detector was a system composed of a high-sensitive videocamera for the visible range and a scintillator, mounted at a distance of 5 cm from the sample. The videocamera used was Hamamatsu ORCA-Flah3.0 with a 2048x2048 matrix, pixel size 6.5x6.5 μm^2, with the dynamic range of 16 bit. The magnification factor of the optical objective mounted on the detector was 4.17, which allowed us to obtain digital images with pixel size 1.56 × 1.56 μm^2. To decrease the noise in the recorded images, the camera was equipped with Peltier element, maintaining the working temperature of the matrix at a level of −20 °C. Gadolinium-aluminum-gallium garnet doped with cerium was used as the scintillator to transform X-ray radiation into the visible range. 10 μm thick garnet single crystal allowed us to obtain X-ray images with the spatial resolution at a level of 3 μm, which was determined using the method described in (Kozyrev et al., 2016). The processing of radiographic images, including the integration of color intensities, was carried out using the ImageJ software (Schneider et al., 2021).

The experimental cell is shown schematically in Fig. 2. The cell is symmetrical with respect to the rotation axis. Sample (1) is loaded in the Caprolon cup (2) with an inner diameter of 7 mm, 4 mm in height, and a wall thickness of less than 0.4 mm. The cup is glued to the sample holder (3). The sample holder is placed in the cell (4) made of PEEK plastic. The outer diameter of the cell is 20 mm, and the inner one is 11 mm. The cell is closed at the ends with caps. Rubber ring sealers provide the tightness of cap contact with the cell. The calculated limiting pressure in the experimental cell is 15 MPa. The cell is thermostated with cold air supplied into the jacket (5). Temperature is controlled with a thermistor (6), placed in the sample holder (3). Gas is supplied using the admission system (7) through a flexible PEEK capillary connected to the gas channel at the top cap of the experimental cell. The pressure is measured with a transducer with the measurement scale of 2.5 MPa.

During experiment preparation, 200 μL of the emulsion was loaded into the cup (1). Then the cell was blown with xenon, and gas pressure was elevated to 1.4 MPa. The emulsion was saturated with xenon for 8 h at +25 °C. The experiment was carried out as follows. The cell was cooled to −4°C at about 0.5 °C/min. The hydrate formation started at −1°C, which caused a temperature rise to +5 °C in the experimental cell. After 40 min, the temperature was stabilized at −4°C. The radiographic recording was carried out with a frame frequency of 1 Hz during the whole experiment.

The Xe hydrate formation was also assessed by high-pressure μDSC7 Evo (Setaram Instrumentation, France). The experimental procedure was the same as for the radiographic measurements. PMHP 56-1000V2 gas panel maintained the constant pressure in the DSC cell.

3. Results and discussion

Typical radiographic images obtained in the experiment are in Fig. 3. All images shown are 2D projections of 3D space (Fig. 2B). In radiographic images taken before hydrate formation (Fig. 3A), oil, water, and gaseous xenon have approximately the same X-ray densities. Due to X-ray refraction, only the meniscus line separating the liquid phase from the gas is clearly detected.

Xenon concentration in the hydrate is about an order of magnitude higher than in the gas phase present in the apparatus. Indeed, it is easy to calculate that 1 cm^3 of gaseous xenon at 1.4 MPa weighs approximately 0.08 g. At the same time, it can be determined from the data of (Hassanpouryouzband et al., 2020; Manakov and Stoporev, 2021; Sloan and Koh, 2007) that 1 cm^3 of hydrate contains 0.88 g of xenon. Since xenon has a much higher electron density than oxygen, carbon, nitrogen and hydrogen, the degree of X-ray absorption by oil, gas and hydrate in our work is primarily determined by xenon content in these phases. In this way, the hydrate formation appears on X-ray images as the shadowed regions so that the intensity of black coloring is proportional to the total hydrate content in this region. It should be emphasized that it is impossible to determine the absolute hydrate content in the sample in our experiments. At the same time, the depth of the black color on the radiographic image is proportional to the hydrate content in the sample. This allows one to determine the relative hydrate content and compare the hydrate spatial distribution in the sample at different times. In this sense, the expression "hydrate content" is used in this work. One should note, that in the field of vision on radiographic images shown in Fig. 3A are visible superimposed bulk oil + hydrate, meniscus slopes, and partially gas phase (marked zone in Fig. 2B), which makes it impossible to determine precisely the hydrate position in the direction parallel to the X-ray beam.

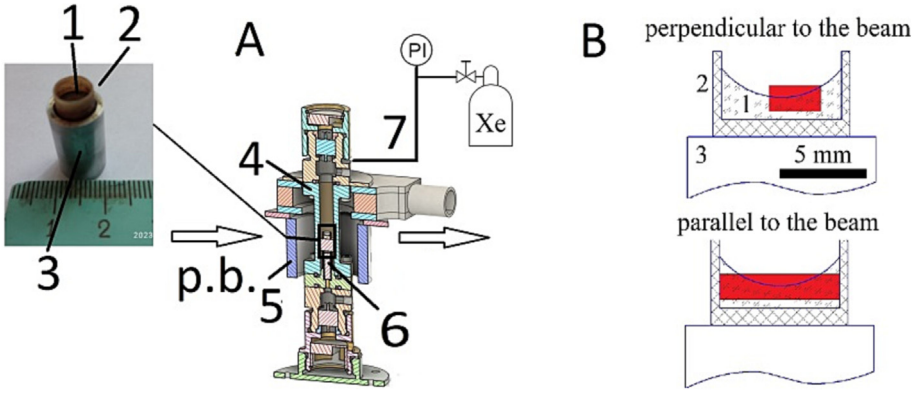

Fig. 2. (A) Scheme of the experimental cell. (1) Sample, (2) caprolon cup, (3) aluminium sample holder, (4) PEEK cell body, (5) cooling jacket, (6) temperature sensor, (7) pressure sensor. p.b. – primary X-ray beam. (B) The areas from which radiological images were taken are marked in red. (For interpretation of the references to color in this figure legend, the reader is referred to the web version of this article.)

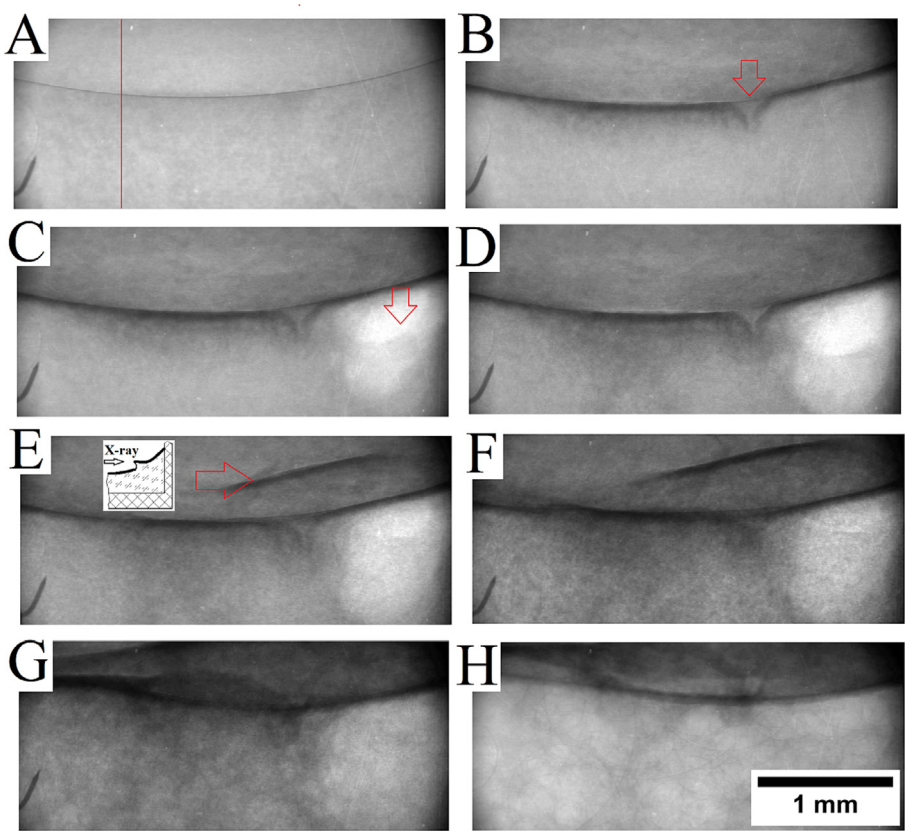

Fig. 3. Radiographic images taken at different stages of the experiment. The time elapsed since the start of hydrate formation is indicated. (A) Before hydrate formation, t = 0 h, the vertical line corresponds to the place where the intensity profiles presented in Fig. 3 were taken; (B) formation of the hydrate at the gas – emulsion boundary, t = 0.18 h; (C) and (D) formation of hydrate and cavity in the bulk of the emulsion, t = 0.40 and 0.65 h, respectively; (E) and (F) further formation of hydrate in the emulsion volume and fracturing on the meniscus, t = 0.79 and 1.65 h, respectively; (G) and (H) decomposition of the hydrate, t = 2.98 and 3.15 h, respectively. For more comments, see the text.

Before the hydrate nucleation, radiographic images corresponded to Fig. 3A. The onset of hydrate formation manifested itself as a small (about 0.1 mm) shift of the emulsion – gas interface and the appearance of a dark strip along this surface (Fig. 3B). The shift of the emulsion – gas interface is caused by the deformation of the sample during the hydrate formation. This will be discussed in more detail below. It is evident that the dark strip corresponds to the zone in which hydrate has been formed, and the intensity of black coloring of this zone is proportional to the amount of hydrate in it. Hereinafter, this zone will be referred to as the hydrate crust. Further, this crust became thicker, and its color became more intense. These processes are well illustrated by the calculated profiles of black color intensity for radiographic images taken at different moments (Fig. 4A). It has already been mentioned that a small peak, which is present on the initial profile at 0 h, corresponds to a narrow dark strip along the meniscus in Fig. 3A, and is caused by X-ray refraction. After the hydrate onset, the width of the peak increases, and the intensity of black coloring at the minimum point increases.

This corresponds to an increase in the hydrate crust thickness and a rise of hydrate (and hence Xe) content in this crust. It should be stressed that a decrease in the numerical values at the vertical axes in Fig. 4 corresponds to an increase in the intensity of the black coloring. The processes took place somewhat differently in different regions of radiographic images. Still, in all cases, an increase in the thickness of the hydrate-saturated layer and increase in color intensity may be divided into two stages – a rapid one, followed by a slow one (Fig. 4B). The duration of the rapid stage was about 190 s (0.053 h). The rate at which the thickness of darkened zone was increasing (thus the rate of the hydrate formation zone propagation) was about 1 μm/s while the slow stage rate was two orders less (about 0.01 μm/s). It should be emphasized that deformation of the emulsion – gas contact surface was observed at this stage, with the formation of a funnel-like defect (indicated with a red arrow in Fig. 3B). Blackening of the zone above the meniscus in Fig. 3B is due to the formation of a layer of subsurface hydrate at the meniscus regions that are sloping concerning the X-ray beam. In general, the rapid hydrate crust growth along the meniscus line may be considered the first stage of hydrate formation when it occurs strictly adjacent to the sample's meniscus region. The slow stage of hydrate crust growth proceeded in parallel with the processes described below. They took place over the whole sample volume, so all these processes together may be assigned to the second stage of the process.

The second stage manifests itself in the central and left parts of the radiographic images by propagating the hydrate formation zone from the meniscus to the lower part of the sample. Hydrate formation proceeded with different intensities at different regions of the pictures, so it is possible to distinguish lighter and darker areas. In all cases, dark spots occurred in light regions (Fig. 3C–F). The characteristic size of these spots was 10–30 μm, so it may be assumed that these spots correspond to coarse emulsion drops on which hydrate crust has been formed. Smaller drops on the images are either invisible, or hydrate formation on them is less probable than on the large ones. The presence of light gaps points to the non-uniformity of hydrate distribution in this area; it seems that the number of coarse drops with the formed hydrates is smaller here. In Fig. 4A, hydrate growth of this kind manifests itself as a

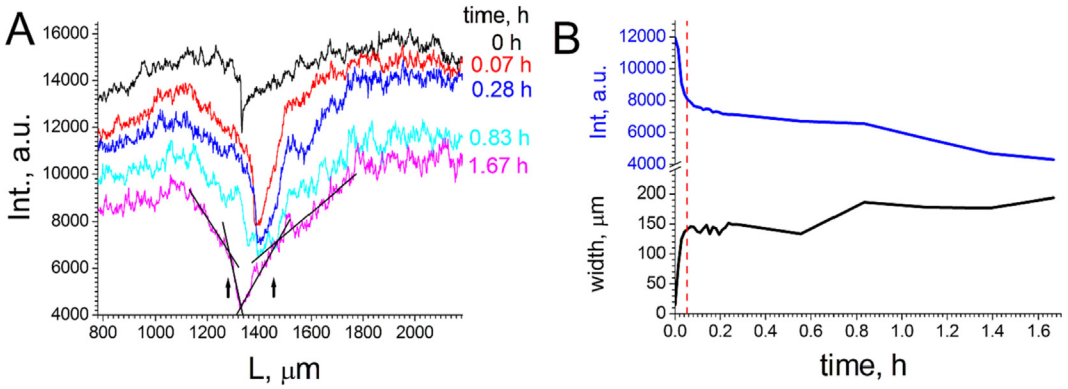

Fig. 4. (a) Vertical intensity profile taken in the position marked in Fig. 3a by red line. 780 μm corresponds to the top of the images presented in Fig. 3. Decrease in the intensity on the vertical axis corresponds to the increase of black colour intensity. (b) Time dependencies of the black colour depth at the profile peak minimum and widths of the peaks. The measuring method for the peak widths is illustrated in the curve 1.67 h of the section (a). The red dashed line corresponds to the boundary between the rapid and slow stages. For more comments see the text. (For interpretation of the references to color in this figure legend, the reader is referred to the web version of this article.)

gradual increase in the extent of black coloring at the background regions of sections.

A light spot appeared in the right part of the radiographic images after approximately 10 min from the hydrate onset. This spot grow within ~15 min (marked with the arrow in Fig. 3C). This is most probably due to a cavity formed in the emulsion because a portion of the emulsion has flowed to a neighboring region or the wall. The appearance of a kind of visor (indicated with the arrow in Fig. 3E) in the same image part, having occurred after the light spot ceased its growth, favors our assumption because this visor may be interpreted as a fragment of the surface hydrate crust forced upward from the meniscus. It may be assumed that the dense hydrate layer located at the position along a slope to the X-ray beam was seen as a uniform darkening prior to the formation of the visor. When the surface layer was fractured, the hydrate crust emerged to the plane parallel to the X-ray beam, which made it visible like the crust on the meniscus discussed above (see insert in Fig. 3E). It seems likely that the fracture of the hydrate crust and sample surface displacement were caused by an increase in the volume of water droplets during hydrate formation. Indeed, it can be readily seen that hydrate volume is larger than the volume of initial water by about 25% (Hassanpouryouzband et al., 2020; Manakov and Stoporev, 2021; Sloan and Koh, 2007). An increase in the volume of hydrate particles compared to the original water drops leads to the appearance of mechanical stresses in the emulsion sample. As a result, deformations and mechanical movement of individual fragments of the emulsion occur. Some transfer of water to the zone of intense hydrate formation also cannot be excluded.

All the above-described events happened about an hour after the start of hydrate formation. During the next two hours, till the end of the experiment, uniform darkening of the whole visible field took place; i.e. the hydrate was formed evenly throughout the entire volume of the sample. In the region of liquid oil emulsion this darkening was dispersed, and light and dark zones were observed, with the characteristic size of dark zones up to 30 μm, as discussed above. During sample heating, hydrate decomposition started in the lower part of the sample. One can see the traces of gas bubbles formed during this process (Fig. 3G,H). These bubbles have driven the solid hydrate crust at the meniscus upward, which may have been partially crushed. The hydrate stayed somewhat monolithic for 10–15 min. This points to the fact that hydrate particles in the crust have grown together, at least partially.

To independently verify the model proposed in this paper, we performed a calorimetric experiment to obtain xenon hydrate from the same emulsion (Fig. 5). The experiment conditions were almost identical to the radiographic study. The emulsion was preliminarily saturated with xenon for 12 h; this stage is not shown in Fig. 5. Further, the temperature was dropped to 3.6 °C, and the sample was kept at this temperature for up to 2 days. Hydrate nucleation manifested as an exothermic effect, with a rapidly growing leading edge and a slowly falling trailing edge. At the leading edge of the exothermic effect, the heat flux continued to grow for 0.048 h, which satisfactorily corresponds to the fast stage of the hydrate formation observed in the X-ray experiment. We assume that the stage of heat flux increase corresponds to the rapid stage of hydrate formation, which corresponds to the growth of the hydrate crust over the sample surface. Next, there is a slow decrease in the heat flux, most likely associated with the transition to a slow stage of hydrate formation (thickening of the hydrate crust, an increase in the hydrate content in the crust, and the formation of hydrate in the bulk of the sample). It should be noted that the trailing edge of the exothermic thermal effect is wide; heat release was recorded for 3 h (Fig. 5). The total amount of heat released was 181.0 J per gram of the sample. After the end of the exothermic effect, the sample was kept at a temperature of −3.6 °C for a day (Fig. 5). At the same time, no thermal effects were observed; the zero line did not demonstrate significant features. Next, the sample was lin-

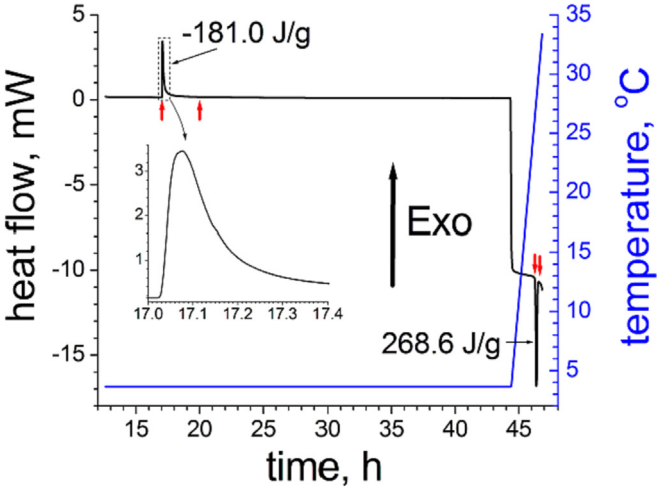

Fig. 5. DSC curve for Xe hydrate formation and decomposition in the water-in-oil emulsion; thermal effects are given per gram of emulsion. The inset shows an enlarged part of the exothermic effect. Red arrows show the boundaries of the exothermic and endothermic effects. (For interpretation of the references to color in this figure legend, the reader is referred to the web version of this article.)

early heated to a temperature of 30 °C. The decomposition of xenon hydrate manifested itself as a single endothermic thermal effect (Fig. 5) with a value of 268.6 J per gram of the sample. Thus, about a third of the decomposed hydrate was formed during 24 h of sample exposure. On the thermal curve, the formation of this hydrate was not clearly manifested. This is in good agreement with the slow formation of hydrate in the sample volume observed on X-ray photographs. Thus, the stages of xenon hydrate formation in the water-in-oil emulsion sample identified in calorimetric experiment are in reasonable agreement with the conclusions drawn from the analysis of X-ray images. Note that the shape of the gas absorption curves reported in the literature (dependence of the amount of gas absorbed into the hydrate on time) also qualitatively corresponds to the presented model (Turner et al., 2009b). The maximum gas absorption rate is observed at the initial stage of the process; further, the gas absorption rate continuously decreases.

4. Conclusions

Thus, our radiographic studies of xenon hydrate formation in water in oil emulsions show that this process follows several stages. The first one is the appearance and rapid growth of the hydrate crust at the gas – emulsion interface. Hydrate content in this crust is the highest over the whole sample. The slow growth of this crust proceeded during the entire experiment. Then, at the second stage of the process, hydrate growth proceeds throughout the emulsion. This growth is non-uniform over the volume, and sometimes accompanied by mechanical deformations of the sample. The growing hydrate is most likely formed as separate grains within the emulsion. In parallel, gradual hydrate growth proceeded within the sample volume. Most probably, that hydrate grains grow together at least partially in the crust formed at the surface of emulsion – gas contact. It may be assumed that differences in hydrate formation in the zone close to the gas – emulsion contact surface and deep in the emulsion are caused by the limited amount of xenon dissolved in oil. Deep in the emulsion, the consumption of xenon dissolved in oil makes hydrate formation stop soon. Its lack is replenished slowly, due to diffusion from the gas phase. Hydrate formation may proceed in this situation either according to the mechanism of the isolated microreactors or according to the relay mechanism, with rapid termination of hydrate formation chains passing between the particles. The process is much faster at the boundary, and the degree of water-to-hydrate transformation is higher due to the rapid recovery of the concentration of gas dissolved in oil. This creates favorable conditions for implementing the relay mechanism of hydrate formation. In general, the features of hydrate formation in quiescent emulsions observed in the current work have some common features with the conceptual models discussed in (Semenov et al., 2015; Stoporev et al., 2019). At the same time, the obtained results provide the possibility of a new look at the localization of hydrate formation areas in emulsions.

CRediT authorship contribution statement

Andrey Yu. Manakov: Conceptualization, Formal analysis, Investigation, Data curation, Writing – original draft, Writing – review & editing. **Konstantin E. Kuper:** Investigation, Methodology. **Arkadi N. Drobchik:** Investigation, Methodology. **Alexey K. Sagidullin:** Investigation. **Matvei E. Semenov:** Investigation. **Andrey S. Stoporev:** Investigation, Writing – review & editing.

Data availability

Data will be made available on request.

Declaration of Competing Interest

The authors declare that they have no known competing financial interests or personal relationships that could have appeared to influence the work reported in this paper.

Acknowledgements

This paper has been supported by the Kazan Federal University Strategic Academic Leadership Program (PRIORITY-2030). The authors are grateful to Dr. T.P. Adamova for help in preparing the figures. The experiments were done at the shared research center SSTRC on the basis of the VEPP-4 - VEPP-2000 complex at BINP SB RAS. Funding: this work was funded by the Ministry of Science and Higher Education of the Russian Federation (grants IPGG SB RAS No. FWZZ-2022-0017 and NIICh SB RAS No. 121031700321-3). DSC study was funded by RFBR, project number 19-35-60013

References

Aman, Z.M., Koh, C.A., 2016. Interfacial phenomena in gas hydrate systems. Chem. Soc. Rev. 45, 1678–1690. https://doi.org/10.1039/c5cs00791g.

Avendaño-Gómez, J.R., Limas-Ballesteros, R., García-Sánchez, F., 2006. Modeling of trichlorofluoromethane hydrate formation in a w/o emulsion submitted to steady cooling. Int. J. Therm. Sci. 45, 494–503. https://doi.org/10.1016/J.IJTHERMALSCI.2005.06.007.

Dalmazzone, D., Hamed, N., Dalmazzone, C., 2009. DSC measurements and modelling of the kinetics of methane hydrate formation in water-in-oil emulsion. Chem. Eng. Sci. 64, 2020–2026. https://doi.org/10.1016/J.CES.2009.01.028.

Handa, Y.P., 1986. Composition dependence of thermodynamic properties of xenon hydrate. J. Phys. Chem. 90, 5497–5498. https://doi.org/10.1021/j100280a002.

Hassanpouryouzband, A., Joonaki, E., Farahani, M.V., Takeya, S., Ruppel, C., Yang, J., English, N.J., Schicks, J.M., Edlmann, K., Mehrabian, H., Aman, Z.M., Tohidi, B., 2020. Gas hydrates in sustainable chemistry. Chem. Soc. Rev. 49, 5225–5309. https://doi.org/10.1039/c8cs00989a.

Hu, S., Koh, C.A., 2017. Interfacial properties and mechanisms dominating gas hydrate cohesion and adhesion in liquid and vapor hydrocarbon phases. Langmuir 33, 11299–11309. https://doi.org/10.1021/acs.langmuir.7b02676.

Istomin, V.A., Yakushev, V.S., 1992. Gazovye Gidraty v Prirodnykh Usloviyakh. (Natural Gas Hydrates). Nedra, Moscow. (in Russian).

Kozyrev, E.A., Kuper, K.E., Lemzyakov, A.G., Petrozhitskiy, A.V., Popov, A.S., 2016. Performance and characterization of CsI: Tl thin films for X-ray imaging application. Phys. Proc. 84, 245–251. https://doi.org/10.1016/J.PHPRO.2016.11.042.

Le, T.-X., Bornert, M., Aimedieu, P., Chabot, B., King, A., Tang, A.-M., 2020. An experimental investigation on methane hydrate morphologies and pore habits in sandy sediment using synchrotron X-ray computed tomography. Mar. Pet. Geol. 122,. https://doi.org/10.1016/j.marpetgeo.2020.104646 104646.

Lv, Y.-N., Sun, C.-Y., Liu, B., Chen, G.-J., Gong, J., 2016. A water droplet size distribution dependent modeling of hydrate formation in water/oil emulsion. AIChE J. 63, 1010–1023. https://doi.org/10.1002/AIC.15436.

Liang, H., Yang, L., Song, Y., Zhao, J., 2021. New approach for determining the reaction rate constant of hydrate formation via X-ray computed tomography. J. Phys. Chem. C 125, 42–48. https://doi.org/10.1021/acs.jpcc.0c07801.

Lv, X., Liu, Y., Shi, B., Zhou, S., Lei, Y., Yu, P., Duan, J., 2020. Study of the comprehensive kinetic model of natural gas hydrate formation in a water-in-oil emulsion flow system. ACS Omega 5, 33101–33112. https://doi.org/10.1021/acsomega.0c04708.

Manakov, A.Y., Stoporev, A.S., 2021. Physical chemistry and technological applications of gas hydrates: topical aspects. Russ. Chem. Rev. 90, 566–600. https://doi.org/10.1070/RCR4986.

Petukhov, A.N., Shablykin, D.N., Trubyanov, M.M., Atlaskin, A.A., Zarubin, D.M., Vorotyntsev, A.V., Stepanova, E.A., Smorodin, K.A., Kazarina, O.V., Petukhova, A. N., Vorotyntsev, V.M., Vorotynstev, I.V., 2022. A hybrid batch distillation/membrane process for high purification. Part 2: Removing of heavy impurities from xenon extracted from natural gas. Sep. Purif. Technol. 294, 121230. doi:10.1016/j.seppur.2022.121230

Pillers, R.A., Heindel, T.J., 2021. Dynamic visualization of hydrate formation using X-ray imaging. J. Pet. Sci. Eng. 200,. https://doi.org/10.1016/J.PETROL.2020.108334 108334.

Pyae, S.N., Grachev, V.M., Dmitrenko, V.V., Ulin, S.E., Vlasik, K.F., Uteshev, Z.M., Shustov, A.E., Novikov, A.S., Petrenko, D.V., Chernysheva, I.V., 2015. Xenon gamma-detector applicability for identification and characterization of radioactive waste. Phys. Proc. 74, 352–356. https://doi.org/10.1016/j.phpro.2015.09.191.

Semenov, M.E., Manakov, A.Y., Shitz, E.Y., Stoporev, A.S., Altunina, L.K., Strelets, L.A., Misyura, S.Y., Nakoryakov, V.E., 2015. DSC and thermal imaging studies of methane hydrate formation and dissociation in water emulsions in crude oils. J.

Therm. Anal. Calorim. 119, 757–767. https://doi.org/10.1007/s10973-014-4203-7.
Sergeeva, M.S., Mokhnachev, N.A., Shablykin, D.N., Vorotyntsev, A.V., Zarubin, D.M., Atlaskin, A.A., Trubyanov, M.M., Vorotyntsev, I.V., Vorotyntsev, V.M., Petukhov, A.N., 2021. Xenon recovery from natural gas by hybrid method based on gas hydrate crystallisation and membrane gas separation. J. Nat.Gas Sci. Eng. 86,. https://doi.org/10.1016/j.jngse.2020.103740 103740.
Schneider, C.A., Rasband, W.S., Eliceiri, K.W., 2021. NIH Image to ImageJ: 25 years of image analysis. Nat. Methods 9 (7), 671–675. https://doi.org/10.1038/nmeth.2089.
Sloan, E.D., Koh, C.A., 2007. Clathrate Hydrates of Natural Gases. CRC Press, Boca Raton.
Sloan, E.D., Koh, C.A., Sum, A.K., 2010. Natural Gas Hydrates in Flow Assurance. Elsevier.
Smetannikov, V.P., Orlov, A.N., Malinin, N.N., Semenova, O.P., 2010. Method of Producing Xenon Concentrate from Natural Combustible Gas, Products of its Treatment Including Man-Caused off Gases and Device to This End (Versions). RU2466086C2.
Stoporev, A.S., Svarovskaya, L.I., Strelets, L.A., Altunina, L.K., Villevald, G.V., Karpova, T.D., Rodionova, T.V., Manakov, A.Y., 2019. Nucleation of methane hydrate and ice in emulsions of water in crude oils and decane under non-isothermal conditions. Chin. J. Chem. Eng. 27, 668–676. https://doi.org/10.1016/J.CJCHE.2018.09.003.
Turner, D.J., Miller, K.T., Sloan, E.D., 2009a. Methane hydrate formation and an inward growing shell model in water-in-oil dispersions. Chem. Eng. Sci. 64, 3996–4004. https://doi.org/10.1016/J.CES.2009.05.051.
Turner, D.J., Miller, K.T., Sloan, E.D., 2009b. Direct conversion of water droplets to methane hydrate in crude oil. Chem. Eng. Sci. 64, 5066–5072. https://doi.org/10.1016/J.CES.2009.08.013.
Uhm, H.S., Oh, P.Y., Choi, E.H., 2008. Properties of excited xenon atoms in an alternating current plasma display panel. Appl. Phys. Lett. 93,. https://doi.org/10.1063/1.3033225 211501.
Wu, Y., Lv, Z., Shang, L., Wang, Z., Liu, B., Wei, L., 2020. The stability and coalescence of hydrate in mineral oil emulsion. Petrol. Sci. Technol. 38, 883–890. https://doi.org/10.1080/10916466.2020.1786117.
Xia, Y., Fang, V., Xu, J., Jia, C., Tao, G., Yu, B., 2018. Clinical efficacy of xenon versus propofol: a systematic review and meta-analysis. Medicine (Baltimore) 97 (20), e10758.
Zhang, J., Li, C., Shi, L., Xia, X., Yang, F., Sun, G., 2022. The formation and aggregation of hydrate in W/O emulsion containing different compositions: a review. Chem. Eng. J. 445,. https://doi.org/10.1016/j.cej.2022.136800 136800.
Zhao, J., Liang, H., Yang, L., Zhang, X., Song, Y., Sum, A.K., 2020. Growth kinetics and gas diffusion in formation of gas hydrates from ice. J. Phys. Chem. C 124, 12999–13007. https://doi.org/10.1021/acs.jpcc.0c03009.